NEUROSCIENCE

In vivo neuromodulation of animal behavior with organic semiconducting oligomers

Giuseppina Tommasini[1]†‡, Mariarosaria De Simone[1]†, Silvia Santillo[1], Gwennaël Dufil[2], Marika Iencharelli[1], Daniele Mantione[3], Eleni Stavrinidou[2], Angela Tino[1], Claudia Tortiglione[1]*

Modulating neural activity with electrical or chemical stimulus can be used for fundamental and applied research. Typically, neuronal stimulation is performed with intracellular and extracellular electrodes that deliver brief electrical pulses to neurons. However, alternative wireless methodologies based on functional materials may allow clinical translation of technologies to modulate neuronal function. Here, we show that the organic semiconducting oligomer 4-[2-{2,5-bis(2,3-dihydrothieno[3,4-b][1,4]dioxin-5-yl)thiophen-3-yl}ethoxy]butane-1-sulfonate (ETE-S) induces precise behaviors in the small invertebrate *Hydra*, which were dissected through pharmacological and electrophysiological approaches. ETE-S–induced behavioral response relies on the presence of head neurons and calcium ions and is prevented by drugs targeting ionotropic channels and muscle contraction. Moreover, ETE-S affects *Hydra*'s electrical activity enhancing the contraction burst frequency. The unexpected neuromodulatory function played by this conjugated oligomer on a simple nerve net opens intriguing research possibilities on fundamental chemical and physical phenomena behind organic bioelectronic interfaces for neuromodulation and on alternative methods that could catalyze a wide expansion of this rising technology for clinical applications.

INTRODUCTION

Recent years have seen major developments of neuroelectronic interfaces aiming to connect the central and peripheral nervous systems to technologies for functional restoration as therapies of neuronal disorders, motor dysfunction, and limb loss. Through varying levels of invasiveness, several types of biomedical devices have been developed to access different forms of neural information, from implantable devices to engineered tissues (*1*, *2*). Ultrathin flexible electronics of disparate geometries and coatings aiming to mimic tissue topography replaced the first generation of stiff and noncompliant neural probes, overcoming mechanical mismatch between neural probes and neuron targets, which can negatively affect native tissue and device performance (*3*, *4*). Bioresorbable and transient electronics, with tunable degradation properties, obviated potential adverse effects of chronic implants and the need for follow-up procedure (*5*). Despite the giant technological advances and the deployment of many devices in the clinical environment, there are still challenges to bridge the gap between the full potential of neuroelectronic interfaces and their translation into broad clinical practice (*6*). Major existing issues are related to methods that enable natural integration of electronic components into neuronal tissue, the timescale of activity, the long-term stability for extended recordings, which would ideally cover the entire adult life of animals, and the availability of models to test in vivo neurostimulation or neuromodulatory action of bioelectronic interfaces (*7*, *8*).

Despite the differences in complexity between the vertebrate and the invertebrate nervous systems, invertebrate models have been proven useful to extract fundamental insights to understand not only basic mechanisms related to neurotransmission and neuroregeneration but also basic principles of bioelectronic communication, neuroscience, and behavior. Millimeter-sized model organisms have also several advantages such as easy manipulation, availability to perform experiments with large numbers of individuals, possibility to dissect anatomical regions, allowing behavioral interrogation in precise location, and absence of ethical concerns, which is an important issue for preclinical testing. Invertebrates have also been largely used for the discovery of neuromodulatory compounds (*9*, *10*). A major obstacle for the discovery of neuroactive compounds is the inability to predict how small molecules will alter complex behaviors. Behavioral profiling in simple animal models may reveal conserved functions of bioactive molecules and predict the mechanisms of action of compounds designed for other purposes (*11*). The small freshwater polyp *Hydra vulgaris* is an attractive animal model for neuromodulation because of its limited behavioral capacity, simple body anatomy, transparency and plasticity of the epithelia, and a nervous system with hundred to thousand neurons (depending on the animal size). Recently, the bioactivity of two organic nanoparticles (NP), based on poly(3-hexylthiophene) (P3HT) and {Poly[2,6-{4,4-bis-(2-ethylhexyl)-4H-cyclopenta [2,1-b;3,4-b′]dithiophene}-alt-4,7(2,1,3-benzothiadiazole)]} polymers, was demonstrated in *Hydra* (*12*, *13*). While both NPs were able to optically modulate tissue regeneration, P3HT-NP could modulate the animal behavior and enhance the expression of genes involved in the light transduction, suggesting a seamless interface between the polymer NP and the living organism (*12*). The light-mediated neuromodulatory function played by P3HT-NP in *Hydra* was also successfully translated to a rat model of retinitis pigmentosa, where P3HT-NP could mediate light-evoked stimulation of retinal neurons and persistently rescue visual functions (*14*).

[1]Istituto di Scienze Applicate e Sistemi Intelligenti "E. Caianiello", Consiglio Nazionale delle Ricerche, Via Campi Flegrei 34, 80078 Pozzuoli, Italy. [2]Laboratory of Organic Electronics, Department of Science and Technology, Linköping University, SE-60174 Norrkoping, Sweden. [3]POLYMAT University of the Basque Country UPV/EHU, 20018 Donostia-San Sebastián, Spain; IKERBASQUE, Basque Foundation for Science, 48009, Bilbao, Spain.
*Corresponding author. Email: claudia.tortiglione@cnr.it
†These authors contributed equally to this work.
‡Present address: Instituto de Nanociencia y Materiales de Aragón (INMA), CSIC-Universidad de Zaragoza, Zaragoza 50018, Spain.

Beside nanostructured and injectable devices, many other geometries and architectures based on organic electronic materials have been proposed to deliver a variety of signals for neuromodulation (*15*), e.g., electrical, physical/piezoelectric, or biochemical stimuli (*7*, *16*), up to built-in conductive devices, produced by the tissue itself starting from chemical inputs. In this latter case, recent pioneering studies demonstrated that the thiophene-based conjugated oligomer 4-[2-{2,5-bis(2,3-dihydrothieno[3,4-b][1,4]dioxin-5-yl)thiophen-3-yl}ethoxy]butane-1-sulfonate (ETE-S) could polymerize in plants, forming conducting wires integrated into the plant structure due to the presence of endogenous peroxidase enzymes (*17*–*19*). In an attempt to translate this phenomenon to an

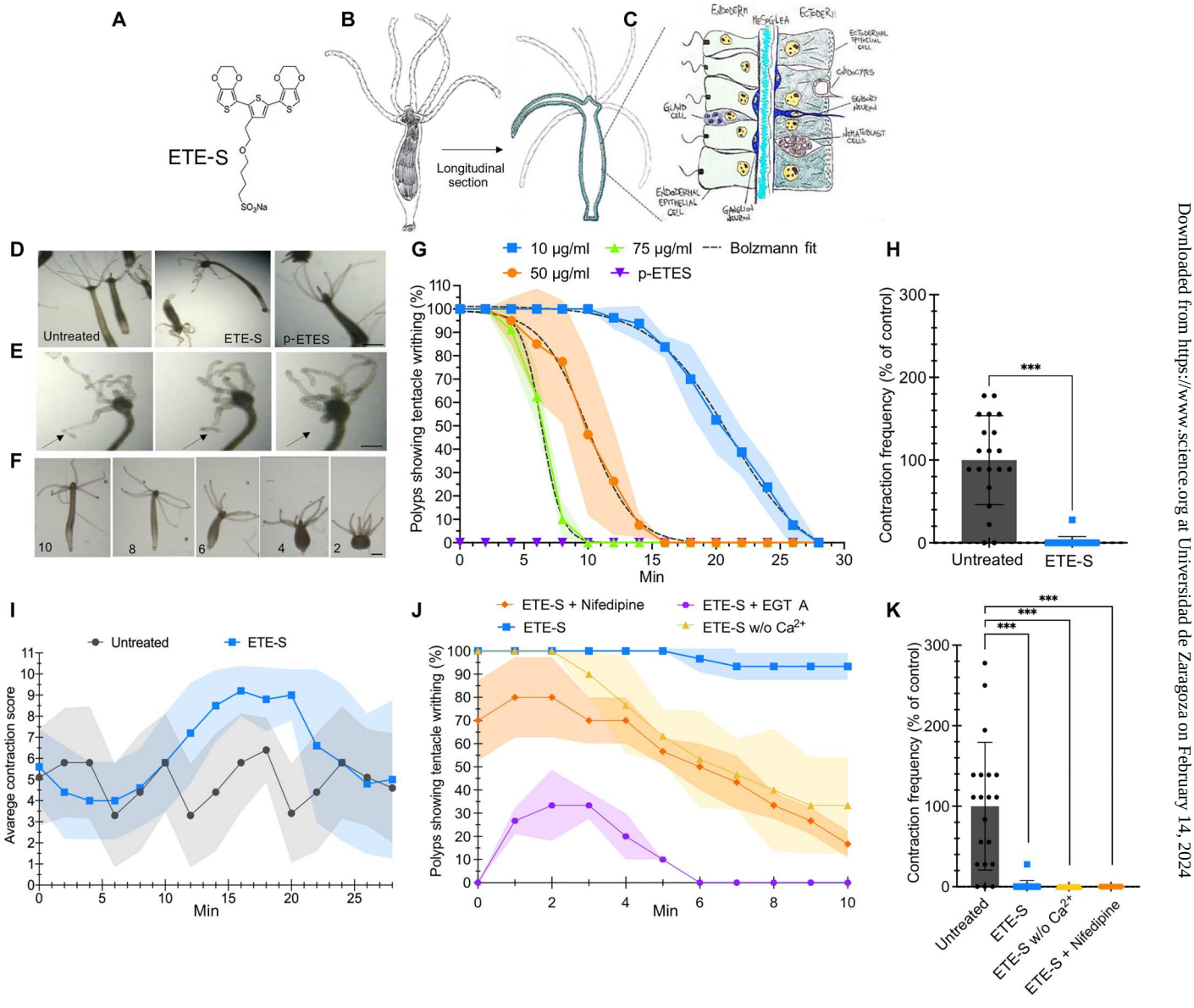

Fig. 1. ETE-S induces a specific behavioral response in *Hydra vulgaris*. (**A**) Molecular structure of ETE-S. (**B**) Schematic representation of *Hydra* body and (**C**) longitudinal section showing the bilayer structure throughout the animal. (**D**) Images of polyps with straight tentacles in normal condition or performing tentacle writhing following ETE-S treatment. pETE-S does not induce any behavior. (**E**) Images showing that each tentacle moves independently from the others (the frames are extracted from movie S2; acquisition time, 1 s); the arrows show the gradual contraction of a single tentacle. (**F**) Images of *Hydra* spontaneous contractions/elongation cycles. Scale bars, 500 µm [(E) and (F)]. (**G**) Temporal dynamic of tentacle writhing at different ETE-S concentrations. SD of mean from four independent replicates ($n = 80$) is shown as a colored halo. The different sigmoidal shape curves were fitted by means of the Boltzmann function (Eq. 1 in Methods). (**H**) ETE-S modulation of body rhythmic contractions. The number of spontaneous contraction/elongation events was monitored over 10 min and compared to untreated individuals ($n = 20$). Unpaired *t* test (two tailed) was used to compare the different conditions. ***$P < 0.001$. (**I**) The contraction pattern was video recorded and transformed into a diagram assigning numerical scores to diverse polyp shapes [shown in (F)]. Experiments were performed in triplicate ($n = 30$). (**J**) Temporal dynamic of ETE-S–induced tentacle writhing in the presence of Ca^{2+} inhibitors. Polyps were pretreated 10 min with the test inhibitors and the behavior monitored for 10 min. SD of mean from three independent replicates ($n = 30$) is shown as a colored halo. (**K**) Modulation of the contraction behavior by Ca^{2+}. Animals treated as in (J) were monitored for the number of contraction/elongation cycles over 10 min after ETE-S addition. Statistical analysis was performed using one-way analysis of variance (ANOVA) and Dunnett's a posteriori test; ***$P < 0.001$.

animal, we found that *Hydra* could also polymerize ETE-S resulting in electronically conducting and electrochemically active micrometer-sized domains fully integrated within the animal tissue. The polymerization was detectable in a specific cell type expressing an endogenous peroxidase as soon as 1 hour after incubation, offering alternative paradigms for in situ production of self-standing electrodes that may be used to stimulate and recording electrical activity (*20*). Recently, in animal models where the native environment is not suitable to promote an efficient ETE-S polymerization because of the lack of peroxidase enzymes, other strategies using ETE analogs and injectable gels have been developed promoting in vivo fabrication of electronic structures triggered by endogenous metabolites (*21*).

While the ETE-S polymerization in *Hydra* was evident, a question that remined unanswered was whether the ETE-S oligomer was inducing any physiological or behavioral response as ETE-S enters the biocatalytic machinery of *Hydra*. Furthermore, investigating the effect of monomers is utmost importance for neural interfaces based on polymers. Long-term stable recordings indeed suffer not only from mechanical and structural disparities between the devices and target tissue but also from stability in the highly oxidant cell environment and from the immune response evoked in the implanted tissue. While these issues are fairly considered, the possibility that polymer degradation products may present unexpected bioactivity is underestimated.

Here, we report that within a few seconds from the addition of ETE-S, an unexpected and peculiar behavior was induced in *Hydra*, consisting in the elicitation of a tentacle-writhing activity and in the modulation of the body column spontaneous contractions. These behaviors were found to be calcium dependent, relying on the presence of head neurons and modulated by several drugs targeting neurons and muscle cells, suggesting possible mechanisms of intracellular transduction of the ETE-S signal. The induced behavior was specific to the ETE trimer as the corresponding polymer p(ETE-S) or 3,4-ethylenedioxythiophene (EDOT) trimers did not induce any response in *Hydra*. Electrophysiological recordings in a whole-animal configuration showed that ETE-S induced the modulation of the *Hydra*'s electrical activity interfering with precise neural networks. Together, our results, spanning from behavioral pharmacology to electrophysiology, show that organic semiconducting molecules could modulate neuronal functions in a simple animal model, pushing toward innovative approaches and wireless solutions for minimally invasive stimulation in vivo.

RESULTS AND DISCUSSION

ETE-S induces a specific behavioral response in *Hydra vulgaris*

The *Hydra* polyp has a very simple structural anatomy; the body is shaped as a hollow tube composed of two epithelial layers, ectoderm and endoderm, separated by an acellular matrix (Fig. 1). An interstitial cell lineage composed of stem cells and a few derivative cell types lies interspersed between these two layers. The nervous system is composed of sensory cells, exposed to the external or gastric environment, and ganglion cells, forming a two-dimensional lattice, also known as nerve net. Initial toxicological evaluation of ETE-S in *Hydra* showed that a treatment with ETE-S within the 10- to 50-μg/ml range is fully biocompatible and does not cause morphological alterations up to 24 hours of continuous incubation (fig. S1), confirming our previous data on ETE-S biocompatibility (*20*). Unexpectedly, immediately after addition of ETE-S to the culture medium hosting the polyps, the tentacle writhing, a behavior usually elicited by live prey, was observed. While untreated polyps soaked in bare *Hydra* medium (HM) exhibited a normal behavior with outstretched and motionless tentacles (Fig. 1D and movie S1), ETE-S addition induced in a few seconds tentacle contractions and bending along the major axis, one independently from the others (Fig. 1E and movie S2). The graph of Fig. 1G reports the temporal dynamic of the tentacle-writhing behavior at different doses. The feature of the responses elicited at any dose are identical, i.e., all the polyps begin the tentacle writhing immediately and the activity ends by a progressive tentacle relaxation back to the normal behavior. The relationship between the ETE-S concentration and the kinetics of the induced response is described with a sigmoidal function with the time constant ($t_{1/2}$) decreasing with increasing ETE-S concentration, i.e., the behavioral response lasts for shorter time in higher dose. This suggest that in higher doses, more ETE-S is binding at the *Hydra* and therefore the induced behavioral response saturates faster.

In addition to the tentacle writhing, the continuous periodic alternation of body contractions and elongations (*22*, *23*) was also modulated by ETE-S, as shown in Fig. 1F. A strong reduction in the frequency of these events, defined as the number of full-body contractions that occurred within 10 min, was observed (Fig. 1H). The contraction pattern was video recorded and transformed into a diagram of polyp shapes, with numerical scores assigned to diverse shapes (Fig. 1F), ranging from 10 (full extension) to 0 (full contraction). The graph of Fig. 1I shows the prolonged contraction of the body column observed in polyps treated with ETE-S along the first 10 min of treatment, followed by an active extension over the following 15 min, shown by the mean contraction profile higher compared to untreated polyps. Overall, these results indicate a clear modulation of the animal contractile behavior.

As *Hydra* is able to polymerize ETE-S (*20*), to investigate whether the bioactive compound was the ETE-S oligomer per se or the resulting polymer in the animal, an in vitro polymerized ETE-S (pETE-S) was tested (*18*, *19*). The treated polyps did not show any behavior in response to the polymer (Fig. 1, D and G, and movie S3), signifying the bioactivity of the thiophene oligomer and in agreement with our previous results indicating that the polymer was detectable only after longer incubation time (1 hour onwards) (*20*). Spectroscopic analysis (fig. S2) performed on treated polyps 10 min after incubation confirmed this hypothesis as detecting a considerable enhancement of the 500-nm absorbance peak (indicating ETE-S polymerization) only in the presence of exogenous H_2O_2.

To establish the biodistribution of the ETE-S into *Hydra* tissues, confocal microscopy was performed on animals treated with ETE-S for 10 min (fig. S3). On the basis of the ETE-S absorption and fluorescence spectra (*17*, *24*), we excited the samples with a λ = 405-nm laser and collected the emission in the range 410 to 488 nm. Fluorescence signal was detected only in treated animals, and it was enhanced at higher ETE-S concentration, especially at the head/tentacle junction region. This suggests that more trimer may bind to the *Hydra* body and agrees with the behavioral response, as the tentacle writhing lasts for shorter time when higher ETE concentration is used.

As it may be argued that the induction and sustainment of the behavioral response over long periods could be due to the degradation or leaching of the trimer from polymerized structures, spectroscopic analysis was performed on the medium incubated 24 hours with polymerized *Hydra* structures. The results showed that no ETE-S trimer is released in the solution as the ETE-S characteristic absorption peak at 350 nm was not present (fig. S4).

The ETE-S–induced behavioral response was also significantly inhibited by H_2O_2 (figs. S5 and S6), possibly also because of the faster polymerization of ETE-S, depleting the free bioactive oligomer. This effect could indicate peroxidase enzymes as transducers of the ETE-S signaling. On the other side, a large number of studies has demonstrated that the H_2O_2 can regulate the neurotransmission acting both as an intracellular signal and as a diffusible messenger (*25*), so we cannot rule out the possibility that H_2O_2 may act as direct neuromodulator in the transduction of ETE-S stimuli.

Furthermore, we found that ETE-S–treated polyps did not respond to a subsequent ETE-S stimulation, performed 1 hour after treatment, suggesting desensitization of a putative target membrane receptor. This observation, together with the absence of effect on normal behaviors (feeding and pinching response) 24 hours after treatment (fig. S7), suggests the occurrence of a neurostimulation process evoked by ETE-S.

ETE-S–induced behaviors are calcium dependent and rely on head neurons

Modulation by calcium

To investigate the role of Ca^{2+} ions in the ETE-S–induced behaviors, both tentacle writhing and body rhythmic contraction were monitored in Ca^{2+}-free medium or by pretreatment with Ca^{2+} chelators, such as EGTA. The results shown in Fig. 1J indicate that in the absence of extracellular Ca^{2+}, the tentacle-writhing activity was strongly inhibited within the first 5 min of treatment, reducing to 60% and to 10% (respectively in Ca^{2+}-free medium and EGTA) the percentage of polyps that still exhibit tentacle writhing. Next, we pharmacologically blocked Ca^{2+} channels that are possibly involved in the intracellular transduction of the ETE-S signaling, such as voltage-dependent L-type Ca^{2+} channels (VDCC) (*26*). After 5-min pretreatment with the well-known organic inhibitor nifedipine (*27*), whose activity in *Hydra* was previously demonstrated (*28*, *29*), only 55% of the polyps were moving and this percentage rapidly decreased to 20% at 10 min (Fig. 1J). Although with slower dynamics compared to the chemical ion chelation, these data confirm the Ca^{2+} involvement in the ETE-S elicited response. In all tested conditions, the polyps responded to ETE-S, but the kinetic profiles of the elicited activities were drastically altered, almost halved in duration. The occurrence of residual tentacle-writhing behavior in the presence of nifedipine or in Ca^{2+}-free medium could suggest the presence of dihydropyridine-insensitive VDCCs or other Ca^{2+}-permeable channels and a role for internal Ca^{2+} stores sufficient to enable, albeit in a limited time interval, the movement of the tentacles (*26*). The inhibitory effects observed in total Ca^{2+} absence or in the presence of chemical chelators suggest a role for Ca^{2+} as a secondary intracellular intermediate in the ETE-S–promoted cascade of events, highlighting that both extracellular and intracellular Ca^{2+} are fundamental to sustain the ETE-S response. The graph of Fig. 1K shows that the frequency of the body rhythmic contractions could be not further modulated in Ca^{2+}-free medium or by nifedipine, as the ETE-S alone was already completely preventing this behavior. Overall, these experiments indicate a strong dependence of all ETE-S–induced behaviors on Ca^{2+}. To explore alternative pathways that could possibly identify the target of the ETE-S–induced response, next we tried to compare it with already characterized behaviors.

Modulation by glutathione

In *Hydra*, the tentacle writhing normally observed during the feeding response can be experimentally induced by reduced glutathione (GSH), used in the micromolar range (*30*, *31*). The behavior is complex and consists of a tentacle-curling activity for an average of 30 min, the opening of the mouth, and the reduction of the body rhythmic activity. The modulation of this behavior represents a robust assay to identify neuroactive compounds and receptors (*32*, *33*). Competition assays performed by monitoring the GSH-induced feeding response in the presence of ETE-S (using equimolar concentration of both compounds) showed a significant inhibition of the tentacle-writhing activity (Fig. 2B). The simultaneous incubation with GSH and ETE-S, indeed, caused a decrease in the percentage of polyps showing tentacle writhing. Fitted curves (fig. S8) show their relative $t_{1/2}$ with that of GSH + ETE-S that unravels an earlier inhibition. In addition, the GSH-induced mouth opening was strongly inhibited by ETE-S, as shown by the complete mouth closure observed in all animals after only 8 min of incubation (Fig. 2C). These results may possibly indicate the same molecular targets shared between ETE-S and GSH on which they could probably exert an antagonist modulatory activity. By decreasing 10 times the ETE-S dose (0.5 μg/ml), the inhibitory effect was still significant, confirming this hypothesis and suggesting a major ETE-S affinity for a target molecule compared to GSH (fig. S9). The effect of the Ca^{2+} was also different between the two induced behaviors. In contrast to the ETE-S case (Fig. 1J), the GSH-induced tentacle writhing was not modulated by the absence of extracellular calcium (fig. S10) within the first 10 min of incubation. This demonstrates a specific rather than general Ca^{2+} involvement in the ETE-S–induced pathway.

Furthermore, we also monitored the modulation of the ETE-S behavior in the presence of a known modulator of the GSH-induced feeding response, i.e., diminazene (*34*). The rationale behind this experiment relies in the capability of this compound to block the *Hydra* Na^+ channel (HyNaC) currents and in vivo to cause a delay of the GSH-induced feeding response, indicating a clear involvement of these peptide-gated channels in the feeding response. Despite belonging to the degenerin/epithelial sodium channel family, these *Hydra* channels differ from vertebrate homologs, as they are highly permeable to Ca^{2+} but are gated by RF-amide (Arg-Phe-NH_2) neuropeptides instead of that by small molecules (*35*–*37*). They are expressed in epithelial cells at the base of the tentacles and in the peduncle and have been suggested playing a role in neuromuscular transmission mediating Ca^{2+} fluxes to depolarize muscle cells and activate muscle contraction. The graphs of Fig. 2 (D and E) show that both ETE-S–induced behaviors were significantly impaired when performed in the presence of diminazene. The tentacle behavior could start (Fig. 2D), but as soon as 5 min after incubation, it was prevented in 65% of polyps, and after 13 min, it was completely blocked. The spontaneous rhythmic contraction behavior was also prevented by diminazene (Fig. 2E), and the strong inhibition inferred by ETE-S did not change in the presence of diminazene. These data suggest that epithelial HyNaC channels

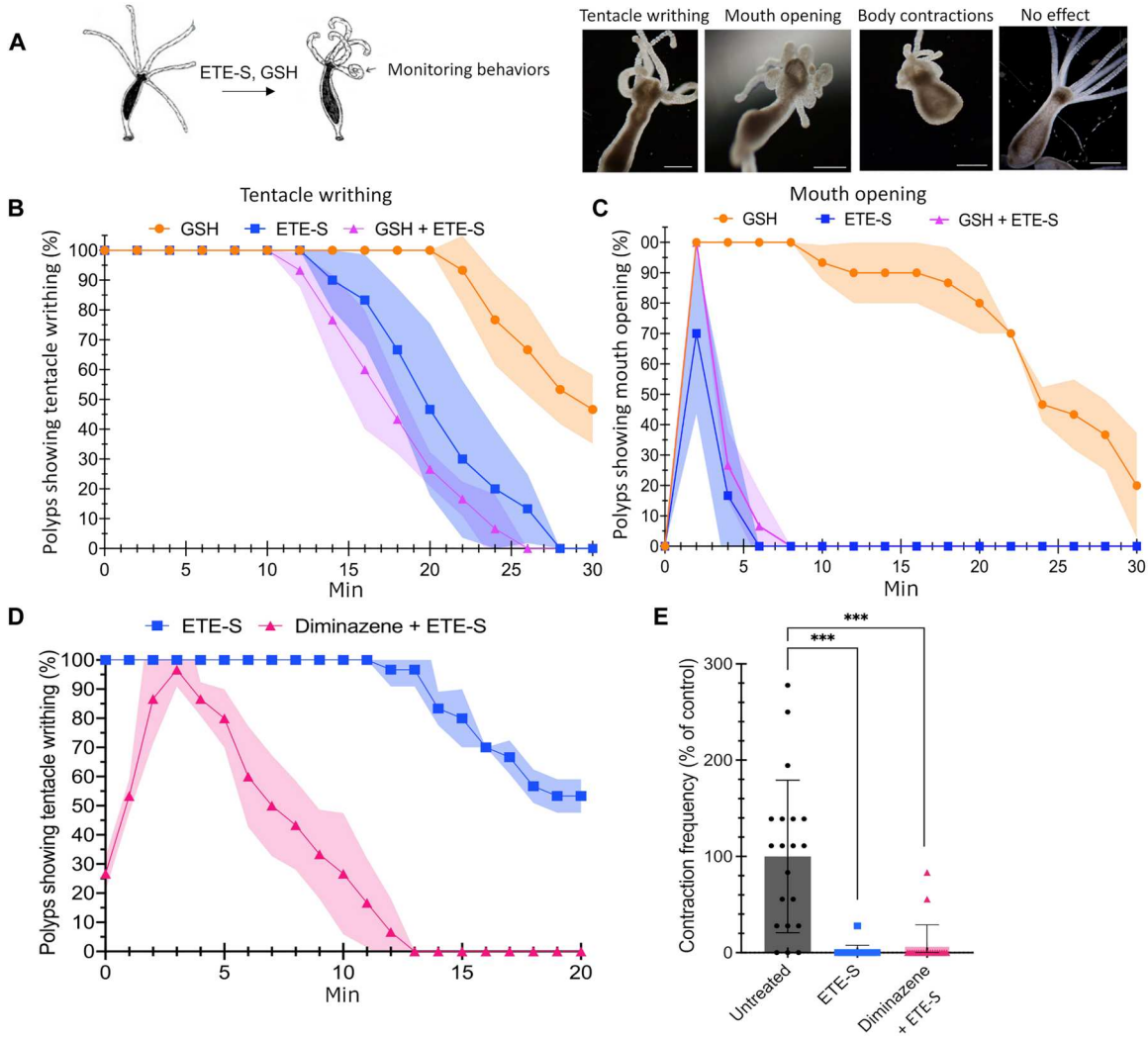

Fig. 2. Modulation of the GSH-induced feeding response by ETE-S. (**A**) Scheme of the experiment. Tentacle writhing and mouth opening represent two distinct behaviors of the feeding response, which is activated by the prey and chemically by reduced GSH. GSH (10 μM) and ETE-S (10 μM) (corresponding to 5.5 μg/ml) were coadministered to living polyps and the behavior monitored for 30 min. (**B**) Temporal dynamic of the GSH-induced tentacle writhing in the presence of ETE-S. The fit to the mean values was performed by the Boltzmann function (fig. S8). (**C**) Temporal dynamic of the GSH-induced mouth opening in the presence of ETE-S. (**D**) *Hydra* polyps were coincubated with ETE-S and diminazene, and the tentacle-writhing activity was monitored at regular intervals. The data are representative of three independent biological replicates and SD of mean from $n = 30$ is shown as a colored halo. (**E**) Modulation of the contraction behavior by diminazene. Animals treated as in (D) were monitored for the number of contraction/elongation cycles over a 10-min period from the ETE-S addition. Statistical analysis ($n = 20$) was performed using one-way ANOVA and Dunnett's a posteriori test; ***$P < 0.001$ compared to untreated polyps.

may be involved in the direct elicitation or in the intracellular transduction of the ETE-S signaling.

Modulation by inhibitor of muscle contraction

With the aim to further dissect the mechanism underlying ETE-S signal transduction, $MgCl_2$ was used, shown in marine invertebrates to prevent muscle contraction (*38*). In *Hydra*, $MgCl_2$ has been used as anesthetic and muscle relaxant, preventing body contraction in response to pinching and the GSH-induced mouth opening by inhibiting ectodermal radial myofibril contraction (*39*, *40*). We found that $MgCl_2$ while at 1% completely prevents the ETE-S–induced tentacle writhing (Fig. 3B and movies S4 and S5), at 0.5% allows the behavior to initiate, and then progressively stops it. A similar effect was observed on the body contraction behavior (Fig. 3C), where the combined presence of $MgCl_2$ and ETE-S has a stronger effect in reducing the contraction frequency compared to the $MgCl_2$ alone but not respect to ETE-S alone. This evidence supports the hypothesis that the ETE-S–induced behaviors are active events driven by contractile processes. To date, the molecular mechanism of myofibril control through the nervous system in *Hydra* is not deciphered yet. However, several pieces of evidence support the presence of neuromuscular junctions, i.e., gap junctions are found connecting neurons and epitheliomuscular cells (*41*) and *Hydra* contractions are greatly reduced in animals chemically depleted of neurons (*42*), suggesting neuron necessity to initiate and to coordinate the muscle activity.

We investigated whether neurons could represent the cellular target of the ETE-S signal by using nerve-free polyps, produced by chemical depletion. First, we evaluated potential toxicity of

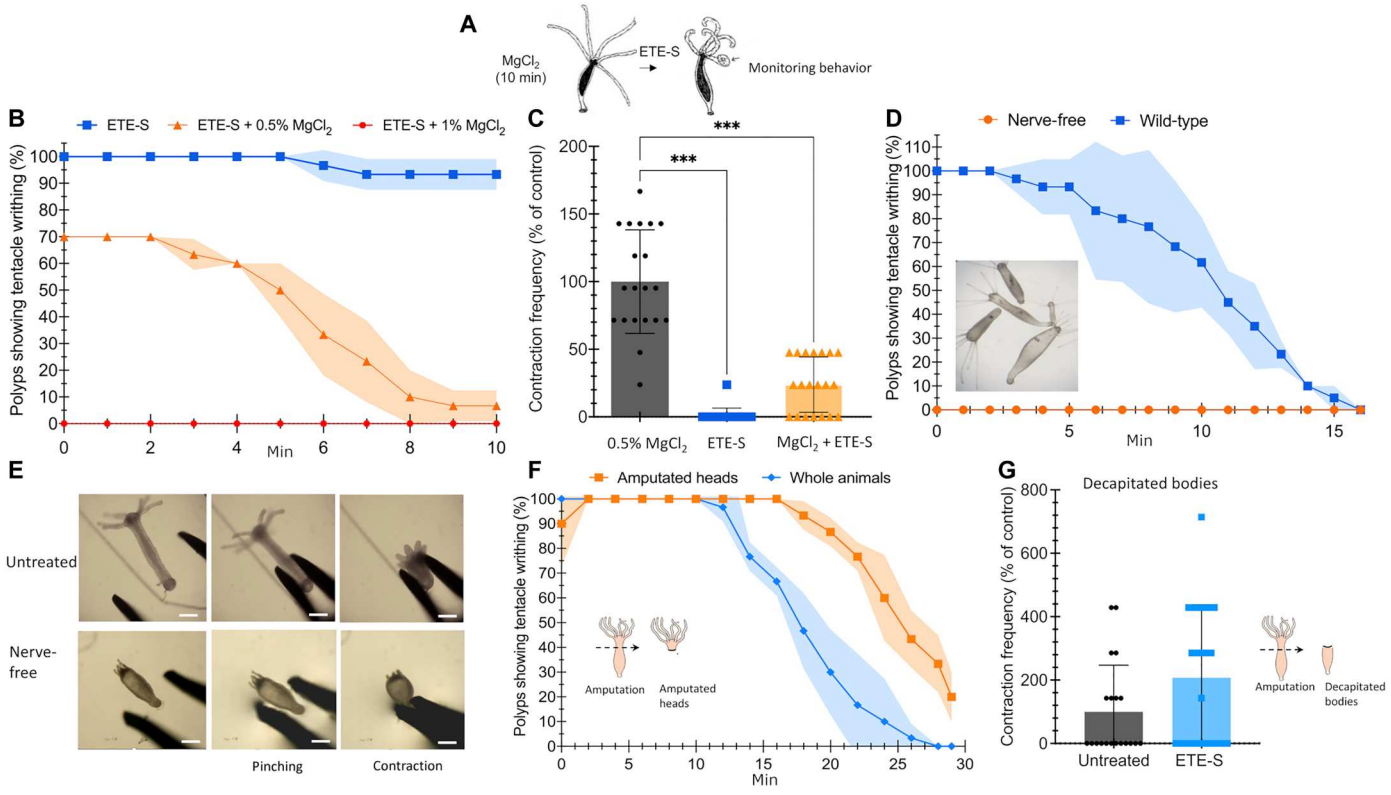

Fig. 3. ETE-S–induced behavior is inhibited by myorelaxant and requires head neurons. (**A**) Scheme of the experiment. Polyps were pretreated 10 min with the indicated dose of $MgCl_2$, then ETE-S (10 μg/ml) was added to the medium, and the induced behaviors were monitored for other 10 min. (**B**) $MgCl_2$ inhibits the ETE-S–induced tentacle writhing. The number of animals showing tentacles writhing was recorded every minute and compared to those treated with ETE-S in the absence of $MgCl_2$. (**C**) Polyps treated as in (A) for the condition of 0.5% $MgCl_2$ dose were video recorded for 10 min and body contraction/elongation events (orange bar) compared to polyps treated with 0.5%$MgCl_2$ alone (gray bar) and ETE-S alone (blue bar). One-way ANOVA followed by Dunnett's test was performed for statistical analysis; ***$P < 0.001$ compared to untreated polyps ($n = 20$). (**D**) The treatment with ETE-S, at 10 μg/ml, does not trigger tentacle-writhing behavior in nerve-free polyps. These polyps (inset images) are still able to contract, as shown in movie S6 and (**E**) after pinching with a forceps, nerve-free polyps show active longitudinal contraction. (**F**) Polyps were amputated, and dissected heads and bodies exposed to ETE-S. The tentacle-writhing activity of isolated heads was longer compared to activity of whole animals, while (**G**) decapitated bodies were not affected by ETE-S; the contraction frequency was not significantly different from untreated samples ($n = 20$). Unpaired *t* test (two tailed) was used for statistical analysis, and no significant differences were detected.

ETE-S on these modified polyps, obtained by colchicine treatment that caused the depletion of the fast-cycling cells, i.e., stem cells and all derivatives, including neurons. No effect was observed on the morphology of polyps at any dose tested, while in normal polyps, doses higher than 50 μg/ml were toxic (fig. S1) suggesting a direct interaction of ETE-S with neurons and nematocytes. When treating nerve-free polyps with ETE-S, we could not detect any behavioral modulation (Fig. 3D), indicating that neurons and not the myofibrils within the epitheliomuscular cells are the direct transducers of the ETE-S signal. It must be noted that in these animals, the spontaneous contraction behavior is abolished, but longitudinal contractions in response to pinching are still possible (Fig. 3E and movie S6) (*40*).

The anatomical dissection of *Hydra* into fully functional heads and bodies (able to regenerate missing parts in a couple of days) lastly allowed us to determinate a physical location of the ETE-S–targeted cells. Amputated heads under ETE-S treatment showed a tentacle-writhing activity identical to that observed in whole animal, which, interestingly, lasted longer compared to whole polyps (Fig. 3F), suggesting a feedback control unit into the rest of the organism. On the contrary, ETE-S was not able to modulate the rhythmic body contractions in decapitated bodies (Fig. 3G), suggesting that the main targets perceiving and transducing the ETE-S signal to other body regions are located on the head, while the gastric and peduncle regions may negatively modulate these responses.

ETE-S induces modulation of *Hydra* electrical activity

In the past, *Hydra* spontaneous and photic behaviors have been associated to extracellular recorded electrical signals, named contraction burst (CB), detected during animal longitudinal contractions, tentacle pulses (TPs) occurring during tentacle contractions, and rhythmic potentials (RP) associated to radial contractions and to a spontaneous electrical activity in the absence of a clear behavior (*43*–*47*). Recently, thanks to breakthrough in Ca^{2+} imaging (i.e., transgenic technology producing animals with cells firing in response to calcium fluxes), these behaviors have been associated to specific neuronal populations (networks) firing simultaneously and located in distinct anatomical regions (*48*). Three major networks structurally and functionally nonoverlapping were identified: an ectodermal CB network underlying longitudinal contractions and two RP networks (one in the ectoderm and one in the endoderm) active

during elongations in response to light and radial contractions, respectively. Beside neuron activity, epitheliomuscular cells contribute to the *Hydra* behavior. These cells, containing myofibrils orthogonally oriented in the ectoderm and endoderm, are excitable, connected through gap junction, and propagate action potentials (*42*, *49*).

To evaluate the relationship among the neuronal and the epitheliomuscular activity and discover whether the ETE-S effect on the *Hydra* behavior could be attributable to neuronal and/or muscular targets, we performed electrophysiological recordings in both normal and nerve-free polyps. Thanks to the soft and deformable *Hydra* epithelial tissues, we were able to carefully suck a small body portion into a glass suction microelectrode and to register its bioelectric activity (Fig. 4A and Methods). The 20-min-long recordings (Fig. 4B) were in agreement with those registered and analyzed by others (*22*, *23*, *44*, *50*). The traces showed high-amplitude electrical events (CBs) occurring at more or less regular intervals conducted by the longitudinal myofibrils of the epitheliomuscular cells and associated to the body contraction behavior (*22*, *48*). The smaller ones (RPs) triggered by the circular myofibril contraction and responsible for the elongation behavior (*44*, *48*, *51*) and those related to the TP from (*52*) were not visible in our traces either in control or in treated animals, probably because of the recording configuration. Figure 4C and fig. S11 show that following ETE-S addition, the rhythmic activity of *Hydra* increased, the intercontraction burst interval (IcBI), i.e., the time interval between the beginning of each two adjacent CB, became shortener and consequently, *Hydra* CB frequency increased. The differences of IcBI mean values between control and ETE-S groups were significant when comparisons were assessed by means of unpaired *t* test (table S1 and Fig. 4D). On the contrary, the recording traces in nerve-free *Hydra* showed the absence of the high-amplitude electrical events, strengthening the current evidence that the *Hydra* neural networks drive its rhythmic behavior (*50*, *53*). The trace profile, in fact, appeared flat except for rarely small-amplitude spikes probably associated to artifacts or to cellular electrogenesis processes not associated to the animal rhythmic activity (Fig. 4E). When adding ETE-S, an upward deflection was detected within few seconds (Fig. 4F and fig. S12), showing that ETE-S could affect the whole contractile machinery and not just the neuronal function.

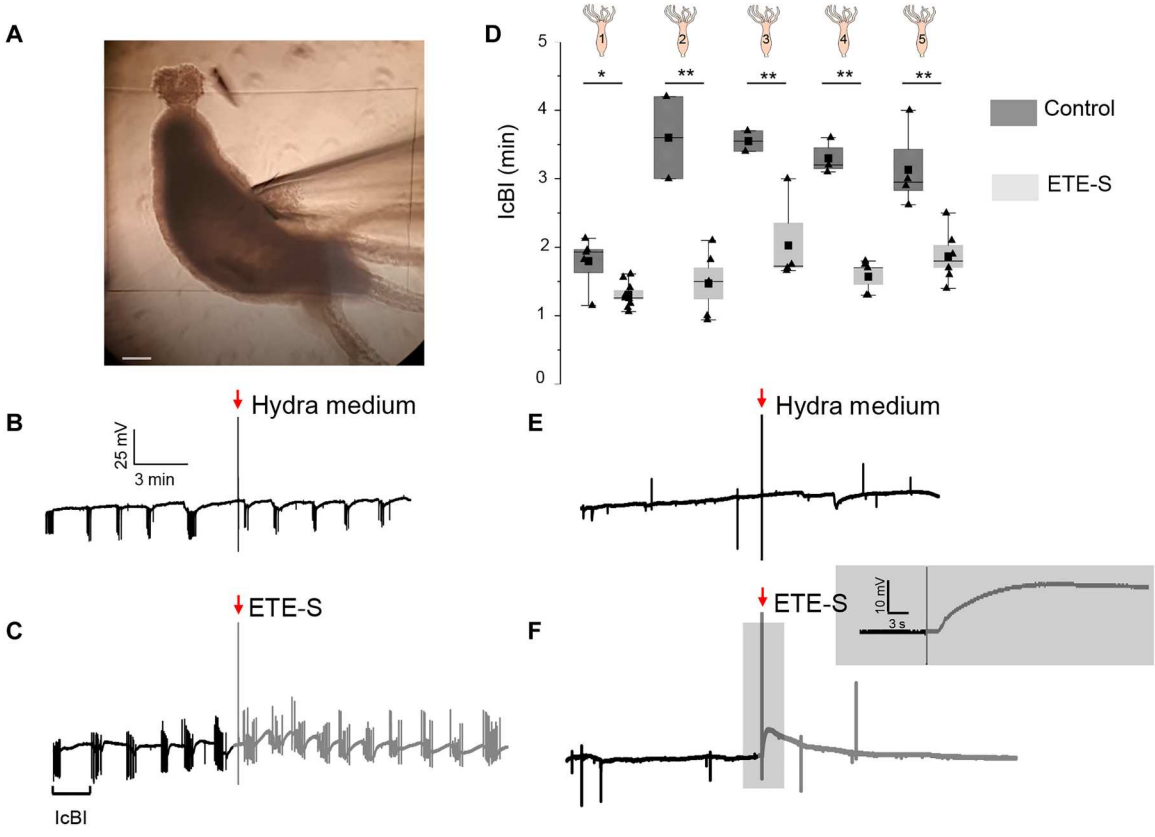

Fig. 4. ETE-S induces modulation on *Hydra* electrical behavior. (**A**) Phase-contrast photomicrographs of a *Hydra* polyp in contact with a glass microelectrode. (**B**) Representative voltage-recording trace demonstrating that the CB activity did not change after injection of 10 μl of *Hydra* medium ($n = 3$). (**C**) ETE-S–induced modulation of *Hydra* rhythmic activity, measured as intercontraction burst intervals (IcBI). CB activity registered 10 min before (black trace) and after (gray trace) injection of 10 μl of ETE-S shows the increase in the CB burst frequency ($n = 5$; fig. S7). (**D**) Box plots depicting mean (black box), median (thin horizontal bar), the 25th and 75th percentiles (shaded boxes), and whiskers showing the 5th and 95th percentiles of the IcBI values, in control and ETE-S groups of five different polyps. Paired *t* test was used for statistical analysis, differences were significant for $^{*}P < 0.05$; $^{**}P < 0.01$. (**E**) Representative recording trace from nerve-free *Hydra* 10 min before and 10 min after injection of 10 μl of *Hydra* medium ($n = 2$). (**F**) Electrical activity of nerve-free polyps in the presence of ETE-S. Recordings acquired 10 min before (black trace) and after (gray trace) injection of ETE-S shows an upward deflection in 2 to 10 s (inset; $n = 5$; fig. S8). All the traces were registered across different animals. The XY scale in (C), (E), and (F) is the same as in (B). Scale bar, 100 μm (A).

ETE-conjugated oligomers act as neuromodulatory compounds

To investigate whether the induced behavioral response is specific to the structure of the ETE-S we incubated *Hydra* polyps with other conjugated oligomers, the ETE-N and EEE-S. ETE-N has the same backbone as ETE-S but a different side chain based on trimethylammonium, while EEE-S has a different backbone, pure EDOT trimer, and same sulphonate side chain as ETE-S (*54*, *55*) (Fig. 5A). Preliminary toxicological tests showed full biocompatibility for both compounds within the first 3 hours of incubation, a period largely extending the time necessary for behavioral studies (i.e., the first 30 min). Longer incubation times were still fully safe for EEE-S while resulting slightly toxic for ETE-N, mirroring the ETE-S toxicological profile (fig. S1). Behavioral experiments performed at the same doses used for ETE-S showed for ETE-N, but not for EEE-S, the elicitation of the tentacle writhing and the inhibition of the spontaneous contraction/elongation activity (Fig. 5, B and C, and movies S6 and S7). In addition, a strong inhibition of the behavioral response in Ca^{2+}-free solution, in the presence of EGTA, and in the presence of VDCC inhibitors (nifedipine) was observed, similarly to ETE-S (Fig. 5D). These results highlight an important role played by the oligomer backbone in the induction of precise behavioral response and strongly suggest specific neuromodulatory action played by these compounds rather than representing generic responses to chemical stimulation. The ETE-N–induced tentacle-writhing activity lasted even longer than the ETE-S–induced behavior, possibly because of different binding/affinity for putative neuroreceptors that can be related to its cationic charge.

Neuromodulation refers to interfacing and intervening with the nervous system through electrical, electromagnetic, chemical, or optogenetic methodologies with the goal of long-term activation, inhibition, modification, and/or regulation of neural activity. It encompasses implantable and nonimplantable technologies, electrical or chemical, for the purpose of improving quality of life and functioning of humans (*15*, *56*, *57*). Here, we report the neuromodulatory function of organic semiconducting compounds on a simple nerve net. Beside the capability to polymerizate into microsized conductive domains that seamlessly integrate into the animal tissues (*20*), ETE-S induced a precise behavioral response, which was thoroughly dissected with behavioral profiling and

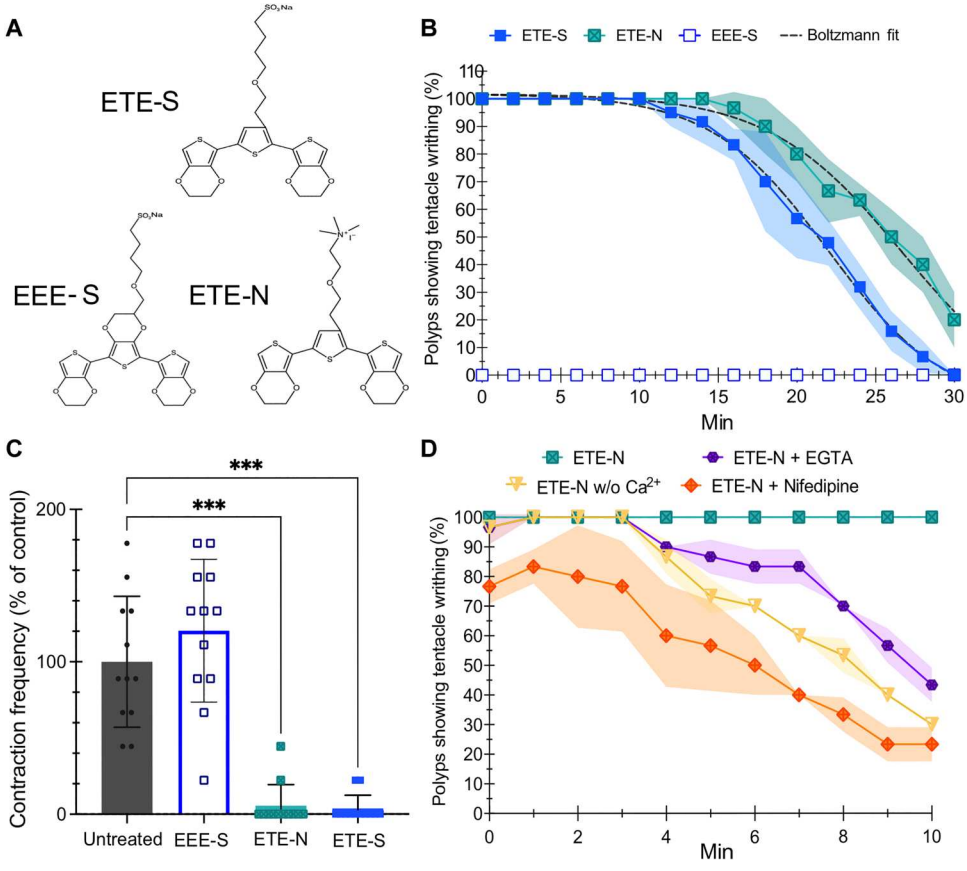

Fig. 5. Stucture-dependent neuromodulatory effect of thiophen-based oligomers. (**A**) Chemical structure of ETE-S, ETE-N, and EEE-S. (**B**) Temporal dynamic of tentacle-writhing behavior induced by 10 μg/ml of ETE-S, compared to ETE-N and EEE-S. Data are the average of three independent experiments, each performed with 10 polyps. The different sigmoidal shape curves were fitted by means of the Boltzmann function (Eq. 1 in Methods). (**C**) Modulation of the spontaneous contraction/elongation events occurring in ETE-S–treated polyps were monitored over 10 min and compared to those occurring in untreated individuals or treated with same dose of EEE-S and ETE-N ($n = 12$). Unpaired t test (two tailed) was used to test comparison between different condition. ***$P < 0.001$. (**D**) Temporal dynamic of ETE-N–induced tentacle writhing in the presence of Ca^{2+} inhibitors. Polyps were pretreated 10 min with the test compound before ETE-S addition to the medium (10 μg/ml) and the induced behavior monitored for 10 min. Data are the average of three independent experiments, each performed with 10 polyps. SD of mean from $n = 30$ is shown as a colored halo.

pharmacological and electrophysiology approaches. ETE-S elicits tentacle-writhing activity and negatively modulates the spontaneous body column contraction events. We found that the ETE-S–induced behavioral response relies on the presence of neurons and Ca^{2+} channels, as it was completely blocked in the absence of Ca^{2+} or in the presence of Ca^{2+} channel inhibitors (nifedipine and diminazene, blocking, respectively, VDCC and HyNaC). Similarities with the GSH-induced feeding response unraveled also other potential ETE-S targets, such as those mediating the GSH-induced response; however, to date they have not been identified. The electrophysiological recordings clearly indicated that ETE-S interferes with the *Hydra* electrical activity may be playing multiple effects on the *Hydra* contractile machinery, i.e., accelerating the CB activity in the ectodermal myofibril system and in tentacles as it results from the increase in the IcBIs, and inhibiting the elongation behavior regulated by RP activity. It must be underlined that by using this electrophysiological configuration, i.e., recording the bulk potential generated by neurons and epitheliomuscular cells, it was not possible to dissect the contributions of the different neuronal networks or of epitheliomuscular cells to these outputs. The recordings on nerve-free polyps allowed us to shed light on this aspect. The abrupt upward voltage deflection registered in these polyps, indeed, represented the hidden ETE-S effect onto the myofibrillar system in the absence of interference of the neural activities. In the presence of neurons, the profoundly different electrical profile of CBs indicates an interaction of ETE-S with the CB neural networks and a modulation of effector myofibrillar system. To date, other than during prey capture, the tentacle-writhing activity can be exogenously induced by GSH (*30*, *31*) while other environmental perturbations such as changes of pH, temperature, light, osmolarity, pressure (*58*–*60*), or the presence of toxicants (*61*, *62*) do not induce such behavior. Only one exception has been documented up to now: the exposure of *Hydra* to metal-based quantum rods (*29*). Investigating the specificity of the ETE-S oligomer, we found that by changing the backbone to a pure EDOT backbone, no behavioral response was induced while oligomers with ETE backbone but bearing different side chains induced a similar response as ETE-S. This reveals a unique feature of ETE-based oligomers to target neuronal activity, rather than reflecting a more general response of the polyp to the changing sensory environment.

Despite recent breakthroughs achieved through Ca^{2+} imaging, allowing to correlate neural or muscle activity to precise behaviors (*58*–*60*, *63*), the correlation between neural and epitheliomuscular

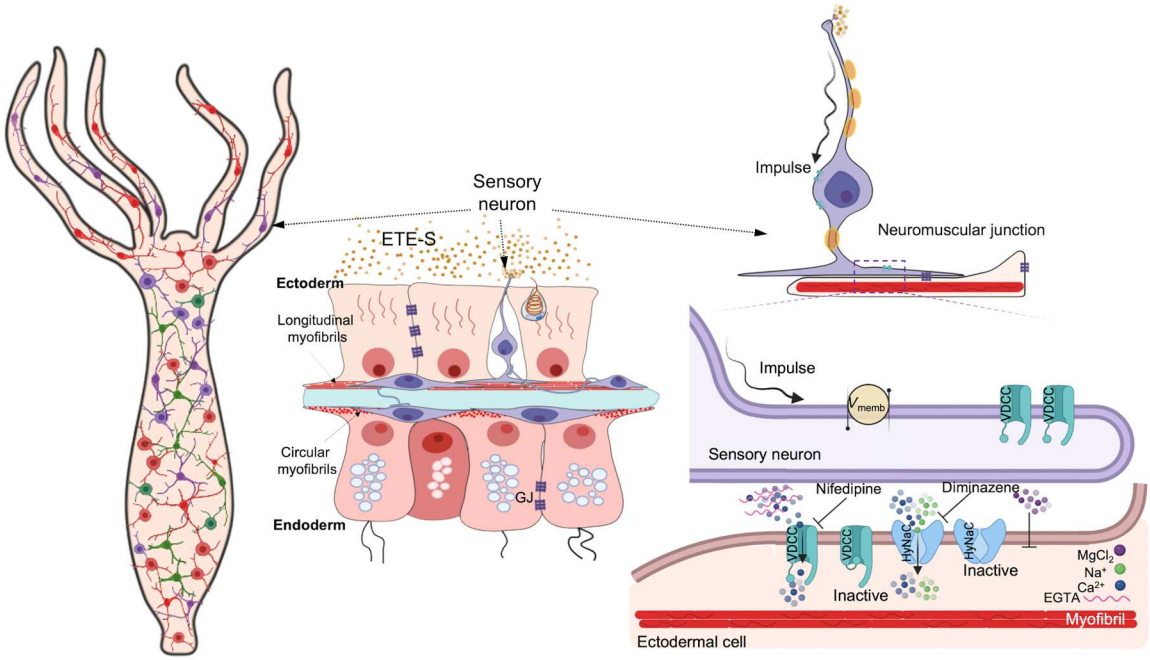

Fig. 6. Mechanism of the ETE-S–induced neuromodulation. Central to the ETE-S neuromodulatory action are the neuronal cells (violet cells), showed as part of the *Hydra* nerve net (left), on the ectodermal epithelium (middle) and interacting with an epitheliomuscular cells (pink cell, right panel). The three main neuronal networks identified by Ca^{2+} imaging are shown extending throughout the entire polyp: one CB (violet net), detected during animal longitudinal contractions, and two RP (green and red nets) associated to radial contractions and spontaneous behavior (*48*). Muscle in *Hydra* consists exclusively of epitheliomuscular cells, generating movement by exerting contractile force via their myofibrils, intercellular muscle processes running longitudinally in the ectoderm (red lines), and circumferentially in the endoderm (red dots). Beside chemical synapsis, stimulus propagation in *Hydra* occurs also through electrical synapsis via gap junctions (GP, violet square), identified between neurons, between epithelial cells (including nematocytes), and between the two (*41*). On the right panel, a possible structure of the neuro-epitheliomuscular junction is depicted with the channels and the chemical modulators tested in this study. VDCC and HyNaC localization are hypothetical but realistic, as calcium channels in the vertebrate synapse are located at both pre- and postsynaptic levels, and HyNaC in *Hydra* are expressed in epitheliomuscular cells, adjacent to RF-amide–producing neurons (*34*). The possible mechanisms of action of ETE-S (yellow dots) involve the interaction with putative metabotropic and/or ionotropic receptors located on sensory neurons and transduced to epitheliomuscular channels on the head. This signaling may modulate Ca^{2+} fluxes causing cell depolarization, acceleration of the CB activity in the ectoderm, and in the tentacles and inhibition of the RP activity. The resulting behaviors consist in the tentacle writhing and in the inhibition of the pulsing behavior. Created with Biorender.com.

cell activity in *Hydra* in response to a physiological or environmental condition has yet to be ruled out. The only direct link between neuron-muscle behavior was found in response to medium osmolarity (*58*). Ca^{2+} imaging showed simultaneous changes in the activity of CB neurons and ectodermal muscle in response to hypo-osmolarity, consistent with the hypothesis that CB neurons activate ectodermal muscle to generate CBs and contractile behavior. In case of ETE-S, a similar activation mechanism of head CB neurons may result in activation of epitheliomuscular cells. The differences in the kinetics of the epitheliomuscular patterns, some propagating quickly in tentacle epitheliomuscular cells and others slowly in body column cells, suggest diverse molecular repertoire involved in each behavior. ETE-S may act as a chemoreceptor ligand and cause the modulation of precise behaviors through several possible mechanisms: (i) ETE-S may act on RF-amide neurons and the signal transduced to ionotropic receptors such as RF-amide–gated Na^+ channels (HyNaC) located in adjacent epitheliomuscular cells (*34*); this is supported by the modulation of the ETE-S response by GSH and diminazene. (ii) A second concomitant possibility is the triggering of VGCC controlling the contraction pulses and TPs, which we identified by using nifedipine and EGTA. Last, (iii) ETE-S action on metabotropic receptors located in the endoderm may explain the modulation of slow behaviors such as body column elongation (*64*). Together, we propose a model of the mechanisms underlying ETE-S–induced neuromodulation (Fig. 6).

We believe that our results, with the limits imposed by behavioral approach and whole-animal electrical recordings, provide important insights on how organic electronic materials can selectively control neuronal activity. The organic chemistry toolbox enables modification of the backbone and side chains (*54*, *55*), offering unique opportunities to develop relationships between structure and induced behavior and to rationally design compounds for targeted neuromodulatory function. While pharmacological techniques represent the oldest and most well-established means for cell-specific neuromodulation, uncovering new modulators to either enhance or diminish the activity of precise neural networks represent a topic of increasing interest in bioelectronics, opening interesting scenarios for the implementation of superior devices. Semiconducting oligomers may be released in situ with miniaturized drug delivery devices for direct neuromodulation activity or integrated in multimodal neuromodulation platforms merging electrical, thermal, optical, and pharmacological stimuli. Last, the simple and limited behavioral repertoire of *Hydra* and the functional conservation of the key neurotransmission mechanisms make *Hydra* an amenable model to identify neuroactive compounds, suggesting application in large-scale screening of innovative neurotechnologies to modulate the nervous system, thus decreasing the need of human exposure for validation of certain tests.

MATERIALS AND METHODS

Synthesis of ETE-S trimer

A detailed description of the synthesis and characterization of the ETE-S, ETE-N, and EEE-S trimers was recently published elsewhere (*55*).

Animal culture

Hydra vulgaris were asexually cultured in *Hydra* medium (HM) (1 mM $CaCl_2$ and 0.1 mM $NaHCO_3$, pH 7), according to the method of Loomis and Lenhoof (*65*). Polyps were fed three times per week with freshly hatched *Artemia salina* nauplii and kept at 18°C with a 12:12-hour light:dark regime. For all the experiments, polyps starved for 24 hours were selected from a homogeneous population.

Evaluation of the ETE-S–induced behavior

Groups of 20 polyps were placed in a plastic multiwell and allowed to equilibrate at room temperature in 300 μl of HM. Behavioral experiments were carried out by adding ETE-S solution at concentration ranging from 75 to 10 μg/ml to each well containing the polyps, and the behavioral activity was monitored using a stereo microscope (Olympus SZX7). The temporal dynamic of ETE-S–induced behavior was quantified by counting the number of polyps showing tentacle activity at 1-min intervals from the beginning of the experiment. Data were expressed as percentage of moving polyps. The experiments were performed at room temperature and repeated three times for each ETE-S concentration tested. Contraction/elongation cycles were monitored on groups of 20 polyps by video recording (JiusionHD 2MP USB Digital Microscope). The number of spontaneous contraction/elongation events occurring in ETE-S–treated polyps were monitored over 10 min and compared to those occurring in untreated individuals. The same method was used to assess bioactivity of ETE-N and EEE-S compounds.

Hydra anatomical dissection

Hydra polyps were bisected subhypostomally, and groups of 10 amputated heads or decapitated bodies were placed in HM and allowed to regenerate for 24 hours before ETE-S addition and monitoring behavioral responses (tentacle writhing and body contraction/elongation cycles) as described above.

Effect of Ca^{2+}

The role played by Ca^{2+} in the ETE-S–induced tentacle writhing was evaluated by performing ETE-S treatment either in Ca^{2+}-free HM or using Ca^{2+} chelators. Groups of 10 polyps were placed in plastic multiwells were pretreated 10 min with 300 μl of HM containing EGTA (4 mM), or with HM containing nifedipine (20 μM), or with Ca^{2+}-free HM (namely, $NaHCO_3$, 0.1 mM) for 1 hour. Following the pretreatment, ETE-S was added to each group of polyps at a final concentration of 10 μg/ml, and polyps were monitored by a stereomicroscope. Control experiments were performed by adding ETE-S (10 μg/ml) to the bathing medium, with no pretreatment. Animal behavior was quantified counting the number of polyps showing tentacle writhing at regular intervals. Data were expressed as percentage of moving polyps. The experiments were repeated three times for each tested condition. The same method was used for ETE-N and EEE-S compounds.

Effect of H_2O_2

The modulation of H_2O_2 on the behavioral response was dissected by carrying out a pretreatment with H_2O_2 excess. A stock solution of H_2O_2 1 M in HM was freshly prepared before each experiment. Each group of polyps was pretreated for 5 min with concentration of H_2O_2 ranging from 1 to 9 mM before ETE-S addition (10 μg/ml). The experiments were repeated three times for each tested condition.

Effect of GSH and other drugs

To prevent the use of oxidized GSH, aliquots of stock solution (GSH, 2 mM) were stored at −20°C and defrost before each experiment. Groups of 10 polyps were coincubated with an equimolar dose of GSH and ETE-S (10 μM), or with excess/defect of 10 times among the two. The dynamics of tentacle writhing and

mouth opening were quantified by counting the number of moving polyps and the number of polyps with open mouth, at 1-min intervals. All the data were expressed as percentages, and the experiments were repeated three times for each tested condition. Polyps treated with GSH (10 μM) alone were used for comparison. The effect of nifedipine as modulator of the feeding response was tested by pretreating the polyps with the drug before adding GSH.

The effect of diminazene, 300 μM as elsewhere reported (*34*), was evaluated by coincubating the polyps with ETE-S, while in case or $MgCl_2$, a 10-min pretreatment with 0.5 and 1% $MgCl_2$ was performed before ETE-S addition (10 μg/ml).

Electrophysiology

Instrumentation setup. Recordings were made by an EPC7 amplifier (HEKA Elektronik) using Digidata 1200A and Clampex8 Software for acquisition. Traces were analyzed with Clampfit10 and Origin2020.

Glass suction microelectrode. Blunt micropipettes with a tip of 150 μm were pulled from a thick-wall borosilicate glass pipette (Sutter catalog no. BF150-86-10) by using a P-1000 micropipette puller (Sutter Instruments). To avoid damages to the animal during the suction, the microelectrode tip border was heat rounded by means of Narishige's MF-79 microforge (Scientific Instrument Lab).

Experimental procedure. Electrophysiological experiments were performed on nonbudding polyps starved for 24 hours and sizing approximatively 1 mm. All recordings took place at 18°C. A glass suction Ag/AgCl microelectrode was gently attached on the animal placed in the recording chamber (1 ml). A portion of the middle part of the body column was sucked into the microelectrode by means of a mild negative pressure applied by a flexible plastic tube connected to the pipette through the electrode holder. Another Ag/AgCl electrode was used as an indifferent one. Animals were allowed to adapt for about 10 min before recordings. *Hydra* medium was used both in the recording chamber and in the glass micropipette.

Statistical analysis and fitting

Data were presented as means ± SD. Two-tailed unpaired *t* test was performed for statistical significance of the mean differences, $^{*}P < 0.05$; $^{**}P < 0.01$; $^{***}P < 0.001$. For multiple comparisons, one-way analysis of variance (ANOVA) and Dunnett's post hoc test were used, $^{***}P < 0.001$.

Electrophysiological data were represented by box-and-whisker plots, with the box depicting the mean, the median (Q_2, thin horizontal bar), the 25th (Q_1) and 75th (Q_3) quartile and the whisker showing the 5th and 95th percentile. Paired *t* test was performed for statistical significance of the mean differences (t_{df} = *t* stat; *P* value) after assessing the equal variance; $^{*}P < 0.05$, $^{**}P < 0.01$, and $^{***}P < 0.001$ were considered statistically significant (Origin 2020 and GraphPad 8).

The curves of graph Fig. 1G were fitted by the following Boltzmann equation

$$Y = A_{\min} + \frac{A_{\max} - A_{\min}}{1 + e^{(x - x_0/k)}} \quad (1)$$

where A_{max} and A_{min} represent the initial and final values of the curves and *k*, expressed in minutes, their steepness. The $t_{1/2}$ (the time at which the behavioral response is inhibited in 50% of polyps) and the related slope factor, *K*, resulted to be respectively 21.09 ± 0.26 and 3.07 ± 0.3 at 10 μg/ml, 9.93 ± 0.14 and 1.82 ± 0.12 at 50 μg/ml, and 6.39 ± 0.04 and 0.78 ± 0.04 at 75 μg/ml.

Supplementary Materials

This PDF file includes:

Figs. S1 to S12
Legends for movies S1 to S8
Table S1
References

Other Supplementary Material for this manuscript includes the following:

Movies S1 to S8

REFERENCES AND NOTES

1. R. Feiner, T. Dvir, Tissue-electronics interfaces: from implantable devices to engineered tissues. *Nat Rev Mater* **3**, 17076 (2018).
2. K. A. Yildiz, A. Y. Shin, K. R. Kaufman, Interfaces with the peripheral nervous system for the control of a neuroprosthetic limb: a review. *J. Neuroeng. Rehabil.* **17**, 43 (2020).
3. Y. X. Liu, J. Liu, S. C. Chen, T. Lei, Y. Kim, S. M. Niu, H. L. Wang, X. Wang, A. M. Foudeh, J. B. H. Tok, Z. N. Bao, Soft and elastic hydrogel-based microelectronics for localized low-voltage neuromodulation. *Nat Biomed Eng* **3**, 58–68 (2019).
4. S. Zhao, X. Tang, W. Tian, S. Partarrieu, R. Liu, H. Shen, J. Lee, S. Guo, Z. Lin, J. Liu, Tracking neural activity from the same cells during the entire adult life of mice. *Nat. Neurosci.* **26**, 696–710 (2023).
5. S. W. Hwang, H. Tao, D. H. Kim, H. Y. Cheng, J. K. Song, E. Rill, M. A. Brenckle, B. Panilaitis, S. M. Won, Y. S. Kim, Y. M. Song, K. J. Yu, A. Ameen, R. Li, Y. W. Su, M. M. Yang, D. L. Kaplan, M. R. Zakin, M. J. Slepian, Y. G. Huang, F. G. Omenetto, J. A. Rogers, A Physically Transient Form of Silicon Electronics. *Science* **337**, 1640–1644 (2012).
6. I. Ezeokafor, A. Upadhya, S. Shetty, Neurosensory Prosthetics: An Integral Neuromodulation Part of Bioelectronic Device. *Front. Neurosci.* **15**, 671767 (2021).
7. M. Berggren, E. D. Glowacki, D. T. Simon, E. Stavrinidou, K. Tybrandt, In Vivo Organic Bioelectronics for Neuromodulation. *Chem. Rev.* **122**, 4826–4846 (2022).
8. D. I. Medagoda, D. Ghezzi, Organic semiconductors for light-mediated neuromodulation. *Commun Mater* **2**, 111 (2021).
9. H. J. Bellen, C. Tong, H. Tsuda, 100 years of Drosophila research and its impact on vertebrate neuroscience: a history lesson for the future. *Nat. Rev. Neurosci.* **11**, 514–522 (2010).
10. J. Rihel, D. A. Prober, A. Arvanites, K. Lam, S. Zimmerman, S. Jang, S. J. Haggarty, D. Kokel, L. L. Rubin, R. T. Peterson, A. F. Schier, Zebrafish behavioral profiling links drugs to biological targets and rest/wake regulation. *Science* **327**, 348–351 (2010).
11. D. L. Gonzales, K. N. Badhiwala, B. W. Avants, J. T. Robinson, Bioelectronics for Millimeter-Sized Model Organisms. *iScience* **23**, 100917 (2020).
12. C. Tortiglione, M. R. Antognazza, A. Tino, C. Bossio, V. Marchesano, A. Bauduin, M. Zangoli, S. V. Morata, G. Lanzani, Semiconducting polymers are light nanotransducers in eyeless animals. *Sci. Adv.* **3**, e1601699 (2017).
13. G. Onorato, F. Fardella, A. Lewinska, F. Gobbo, G. Tommasini, M. Wnuk, A. Tino, M. Moros, M. R. Antognazza, C. Tortiglione, Optical Control of Tissue Regeneration through Photostimulation of Organic Semiconducting Nanoparticles. *Adv. Healthc. Mater.* **11**, e2200366 (2022).
14. J. F. Maya-Vetencourt, G. Manfredi, M. Mete, E. Colombo, M. Bramini, S. Di Marco, D. Shmal, G. Mantero, M. Dipalo, A. Rocchi, M. L. DiFrancesco, E. D. Papaleo, A. Russo, J. Barsotti, C. Eleftheriou, F. Di Maria, V. Cossu, F. Piazza, L. Emionite, F. Ticconi, C. Marini, G. Sambuceti, G. Pertile, G. Lanzani, F. Benfenati, Subretinally injected semiconducting polymer nanoparticles rescue vision in a rat model of retinal dystrophy. *Nat. Nanotechnol.* **15**, 698 (2020).
15. S. M. Won, E. Song, J. T. Reeder, J. A. Rogers, Emerging Modalities and Implantable Technologies for Neuromodulation. *Cell* **181**, 115–135 (2020).
16. S. Luan, I. Williams, K. Nikolic, T. G. Constandinou, Neuromodulation: present and emerging methods. *Front Neuroeng* **7**, 27 (2014).
17. E. Stavrinidou, R. Gabrielsson, K. P. Nilsson, S. K. Singh, J. F. Franco-Gonzalez, A. V. Volkov, M. P. Jonsson, A. Grimoldi, M. Elgland, I. V. Zozoulenko, D. T. Simon, M. Berggren, In vivo polymerization and manufacturing of wires and supercapacitors in plants. *Proc. Natl. Acad. Sci. U.S.A.* **114**, 2807–2812 (2017).
18. D. Parker, Y. Daguerre, G. Dufil, D. Mantione, E. Solano, E. Cloutet, G. Hadziioannou, T. Nasholm, M. Berggren, E. Pavlopoulou, E. Stavrinidou, Biohybrid plants with electronic roots via in vivo polymerization of conjugated oligomers. *Mater Horiz* **8**, 3295–3305 (2021).

19. G. Dufil, D. Parker, J. Y. Gerasimov, T. Q. Nguyen, M. Berggren, E. Stavrinidou, Enzyme-assisted in vivo polymerisation of conjugated oligomer based conductors. *J. Mater. Chem. B* **8**, 4221–4227 (2020).
20. G. Tommasini, G. Dufil, F. Fardella, X. Strakosas, E. Fergola, T. Abrahamsson, D. Bliman, R. Olsson, M. Berggren, A. Tino, E. Stavrinidou, C. Tortiglione, Seamless integration of bioelectronic interface in an animal model via in vivo polymerization of conjugated oligomers. *Bio Mater* **10**, 107–116 (2022).
21. X. Strakosas, H. Biesmans, T. Abrahamsson, K. Hellman, M. S. Ejneby, M. J. Donahue, P. Ekstrom, F. Ek, M. Savvakis, M. Hjort, D. Bliman, M. Linares, C. Lindholm, E. Stavrinidou, J. Y. Gerasimov, D. T. Simon, R. Olsson, M. Berggren, Metabolite-induced in vivo fabrication of substrate-free organic bioelectronics. *Science* **379**, 795–802 (2023).
22. L. M. Passano, C. B. McCullough, Co-Ordinating Systems and Behaviour in Hydra. *J. Exp. Biol.* **41**, 643–664 (1964).
23. C. Taddeiferretti, L. Cordella, Modulation of Hydra Attenuata Rhythmic Activity - Photic Stimulation. *Arch. Ital. Biol.* **113**, 107–121 (1975).
24. A. V. Volkov, S. K. Singh, E. Stavrinidou, R. Gabrielsson, J. F. Franco-Gonzalez, A. Cruce, W. M. Chen, D. T. Simon, M. Berggren, I. V. Zozoulenko, Spectroelectrochemistry and Nature of Charge Carriers in Self-Doped Conducting Polymer. *Adv Electron Mater* **3**, 1700096 (2017).
25. M. E. Rice, H2O2: A dynamic neuromodulator. *Neuroscientist* **17**, 389–406 (2011).
26. A. Senatore, H. Raiss, P. Le, Physiology and Evolution of Voltage-Gated Calcium Channels in Early Diverging Animal Phyla: Cnidaria, Placozoa, Porifera and Ctenophora. *Porifera and Ctenophora. Front Physiol* **7**, 481 (2016).
27. A. Senatore, A. Boone, S. Lam, T. F. Dawson, B. Zhorov, J. D. Spafford, Mapping of dihydropyridine binding residues in a less sensitive invertebrate L-type calcium channel (LCa v 1). *Channels (Austin)* **5**, 173–187 (2011).
28. W. Vater, G. Kroneberg, F. Hoffmeister, H. Saller, K. Meng, A. Oberdorf, W. Puls, K. Schlossmann, K. Stoepel, [Pharmacology of 4-(2'-nitrophenyl)-2,6-dimethyl-1,4-dihydropyridine-3,5-dicarboxylic acid dimethyl ester (Nifedipine, BAY a 1040)]. *Arzneimittelforschung* **22**, 1–14 (1972).
29. M. A. Malvindi, L. Carbone, A. Quarta, A. Tino, L. Manna, T. Pellegrino, C. Tortiglione, Rod-shaped nanocrystals elicit neuronal activity in vivo. *Small* **4**, 1747–1755 (2008).
30. H. M. Lenhoff, "Biology and physical chemistry of feeding response of hydra" in *Biochemistry of Taste and Olfaction*, R. H. Cagan, M. R. Kare, Eds. (Academic Press, 1981), pp. 457–497.
31. W. F. Loomis, Glutathione control of the specific feeding reactions of hydra. *Ann. N. Y. Acad. Sci.* **62**, 209 (1955).
32. P. Pierobon, Regional modulation of the response to glutathione in Hydra vulgaris. *J. Exp. Biol.* **218**, 2226–2232 (2015).
33. P. Pierobon, C. Sogliano, R. Minei, A. Tino, P. Porcu, G. Marino, C. Tortiglione, A. Concas, Putative NMDA receptors in Hydra: a biochemical and functional study. *Eur. J. Neurosci.* **20**, 2598–2604 (2004).
34. M. Assmann, A. Kuhn, S. Durrnagel, T. W. Holstein, S. Grunder, The comprehensive analysis of DEG/ENaC subunits in Hydra reveals a large variety of peptide-gated channels, potentially involved in neuromuscular transmission. *BMC Biol.* **12**, 84 (2014).
35. A. Golubovic, A. Kuhn, M. Williamson, H. Kalbacher, T. W. Holstein, C. J. Grimmelikhuijzen, S. Grunder, A peptide-gated ion channel from the freshwater polyp Hydra. *J. Biol. Chem.* **282**, 35098–35103 (2007).
36. S. Durrnagel, A. Kuhn, C. D. Tsiairis, M. Williamson, H. Kalbacher, C. J. P. Grimmelikhuijzen, T. W. Holstein, S. Grunder, Three Homologous Subunits Form a High Affinity Peptide-gated Ion Channel in Hydra. *J. Biol. Chem.* **285**, 11958–11965 (2010).
37. O. Koizumi, J. D. Wilson, C. J. Grimmelikhuijzen, J. A. Westfall, Ultrastructural localization of RFamide-like peptides in neuronal dense-cored vesicles in the peduncle of Hydra. *J. Exp. Zool.* **249**, 17–22 (1989).
38. M. J. Abrams, T. Basinger, W. Yuan, C. L. Guo, L. Goentoro, Self-repairing symmetry in jellyfish through mechanically driven reorganization. *P Natl Acad Sci USA* **112**, E3365–E3373 (2015).
39. J. A. Carter, C. Hyland, R. E. Steele, E. M. Collins, Dynamics of Mouth Opening in Hydra. *Biophys. J.* **110**, 1191–1201 (2016).
40. T. Goel, R. Wang, S. Martin, E. Lanphear, E. M. S. Collins, Linalool acts as a fast and reversible anesthetic in Hydra. *PLOS ONE* **14**, e0224221 (2019).
41. J. A. Westfall, J. C. Kinnamon, D. E. Sims, Neuro-epitheliomuscular cell and neuro-neuronal gap junctions in Hydra. *J. Neurocytol.* **9**, 725–732 (1980).
42. R. D. Campbell, R. K. Josephson, W. E. Schwab, N. B. Rushforth, Excitability of nerve-free hydra. *Nature* **262**, 388–390 (1976).
43. L. M. Passano, C. B. McCullough, The light response and the rhythmic potentials of Hydra. *Natl. Acad. Sci. USA* **48**, 1376–1382 (1962).
44. L. M. Passano, C. B. McCullough, Co-ordinating systems and behaviour in Hydra. *J. Exp. Biol.* **42**, 205–231 (1965).
45. G. Kass-Simon, Longitudinal conduction of contraction burst pulses from hypostomal excitation loci in Hydra attenuata. *J. Comp. Physiol.* **80**, 29–49 (1972).
46. G. Kass-Simon, L. M. Passano, A neuropharmacological analysis of the pacemakers and conducting tissues of Hydra attenuata. *J. Comp. Physiol.* **128**, 71–79 (1978).
47. N. B. Rushforth, D. S. Burke, Behavioral and electrophysiological studies of hydra. II. Pacemaker Activity of Isolated Tentacles. *Biol. Bull.* **140**, 502–519 (1971).
48. C. Dupre, R. Yuste, Non-overlapping Neural Networks in Hydra vulgaris. *Curr. Biol.* **27**, 1085–1097 (2017).
49. R. K. Osephson, M. Macklin, Electrical properties of the body wall of Hydra. *J. Gen. Physiol.* **53**, 638–665 (1969).
50. K. N. Badhiwala, D. L. Gonzales, D. G. Vercosa, B. W. Avants, J. T. Robinson, Microfluidics for electrophysiology, imaging, and behavioral analysis of Hydra. *Lab Chip* **18**, 2523–2539 (2018).
51. G. A. Shibley, Gastrodermal Contractions Correlated with Rhythmic Potentials and Prelocomotor Bursts in Hydra. *Am. Zool.* **9**, 586 (1969).
52. G. Kass-Simon, A. Pannaccione, P. Pierobon, GABA and glutamate receptors are involved in modulating pacemaker activity in hydra. *Comp. Biochem. Physiol. A Mol. Integr. Physiol.* **136**, 329–342 (2003).
53. A. Klimovich, S. Giacomello, A. Bjorklund, L. Faure, M. Kaucka, C. Giez, A. P. Murillo-Rincon, A. S. Matt, D. Willoweit-Ohl, G. Crupi, J. de Anda, G. C. L. Wong, M. D'Amato, I. Adameyko, T. C. G. Bosch, Prototypical pacemaker neurons interact with the resident microbiota. *P Natl Acad Sci USA* **117**, 17854–17863 (2020).
54. L. Vallan, E. Istif, I. J. Gomez, N. Alegret, D. Mantione, Thiophene-Based Trimers and Their Bioapplications: An Overview. *Polymers (Basel)* **13**, (2021).
55. D. Mantione, E. Istif, G. Dufil, L. Vallan, D. Parker, C. Brochon, E. Cloutet, G. Hadziioannou, M. Berggren, E. Stavrinidou, E. Pavlopoulou, Thiophene-Based Trimers for In Vivo Electronic Functionalization of Tissues. *Acs Appl Electron Ma* **2**, 4065–4071 (2020).
56. B. Dhunusmita, D. Nikita, S. Srijani, B. K. Bibhuti, V. Catherine, Neuromodulatory effect of plant metabolites. *Sci Phytochem* **1**, 47–69 (2022).
57. E. S. Krames, P. Hunter Peckham, A. R. Rezai, F. Aboelsaad, in *Neuromodulation*. E. S. Krames, P. Hunter Peckham, A. R. Rezai, Eds. (Academic Press, 2009), pp. 3–8.
58. W. Yamamoto, R. Yuste, Whole-Body Imaging of Neural and Muscle Activity during Behavior in Hydra vulgaris: Effect of Osmolarity on Contraction Bursts. *eNeuro* **7**, ENEURO.0539–ENEU19.2020 (2020).
59. J. R. Szymanski, R. Yuste, Mapping the Whole-Body Muscle Activity of Hydra vulgaris. *Curr. Biol.* **29**, 1807–1817.e3 (2019).
60. K. N. Badhiwala, A. S. Primack, C. E. Juliano, J. T. Robinson, Multiple neuronal networks coordinate Hydra mechanosensory behavior. *eLife* **10**, (2021).
61. M. Allocca, L. Mattera, A. Bauduin, B. Miedziak, M. Moros, L. De Trizio, A. Tino, P. Reiss, A. Ambrosone, C. Tortiglione, An Integrated Multilevel Analysis Profiling Biosafety and Toxicity Induced by Indium- and Cadmium-Based Quantum Dots in Vivo. *Environ. Sci. Technol.* **53**, 3938–3947 (2019).
62. V. Marchesano, A. Ambrosone, J. Bartelmess, F. Strisciante, A. Tino, L. Echegoyen, C. Tortiglione, S. Giordani, Impact of Carbon Nano-Onions on Hydra vulgaris as a Model Organism for Nanoecotoxicology. *Nanomaterials (Basel)* **5**, 1331–1350 (2015).
63. C. N. Tzouanas, S. Kim, K. N. Badhiwala, B. W. Avants, J. T. Robinson, Hydra vulgaris shows stable responses to thermal stimulation despite large changes in the number of neurons. *Iscience* **24**, 102490 (2021).
64. T. Takahashi, Y. Kobayakawa, Y. Muneoka, Y. Fujisawa, S. Mohri, M. Hatta, H. Shimizu, T. Fujisawa, T. Sugiyama, M. Takahara, K. Yanagi, O. Koizumi, Identification of a new member of the GLWamide peptide family: physiological activity and cellular localization in cnidarian polyps. *Comp. Biochem. Physiol. B Biochem. Mol. Biol.* **135**, 309–324 (2003).
65. W. F. Loomis, H. M. Lenhoff, Growth and sexual differentiation of Hydra in mass culture. *J. Exp. Zool.* **132**, 555–573 (1956).
66. H. Sies, Hydrogen peroxide as a central redox signaling molecule in physiological oxidative stress: Oxidative eustress. *Redox Biol.* **11**, 613–619 (2017).

Acknowledgments: We thank F. Fardella for help with manual drawing. Figure 6 was created with Biorender.com. **Funding:** C.T. acknowledges partial support by Air Force Office of Scientific Research, grant no. FA8655-22-1-7014 (LiveSens) and partial support by the European Research Council (ERC) under the European Union's Horizon 2020 research and innovation program "LINCE," grant agreement no. 803621 (C.T. acting as the third party). E.S. and G.D. were funded by the European Union (ERC-2021-STG, 4DPhytoHybrid, 101042148) and by the Swedish Government Strategic Research Area in Materials Science on Advanced Functional Materials at Linköping University (Faculty Grant SFO-Mat-LiU no. 2009-00971). **Author contributions:** Conceptualization: C.T., A.T., and E.S. Methodology: C.T., A.T., E.S., G.T., M.D.S., S.S., and G.D. Investigation: G.T., M.D.S., G.D., D.M., M.I., and S.S. Visualization: C.T., G.T., and S.S. Funding acquisition: C.T. Writing—original draft: C.T. and G.T. Writing—review and editing: C.T., G.T., E.S., S.S., A.T., G.D., D.M., M.I., and M.D.S. Supervision: C.T., A.T., and E.S. **Competing interests:** The

authors declare that they have no competing interests. **Data and materials availability:** All data needed to evaluate the conclusions in the paper are present in the paper and/or the Supplementary Materials.

Submitted 3 May 2023
Accepted 8 September 2023
Published 18 October 2023
10.1126/sciadv.adi5488